Natural convection in an inclined enclosure containing internal energy sources and cooled from below

S. Acharya*

Natural convection in an inclined enclosure cooled from below and containing internally heated fluid has been investigated using a finite difference calculation procedure. Results have been obtained for Rayleigh number values up to 10^6 and for inclination angles of 30 and 60°. For internal Rayleigh numbers that are much larger than the external Rayleigh number, the flow rises in the interior and moves down both the hot and cold walls. On the other hand, if the external Rayleigh number has a larger magnitude, the flow moves upwards along the hot surface and downwards along the cold surface. For the latter situation, the inner core is multi-cellular in nature at large external Rayleigh numbers. The average heat flux ratio along the cold surface (convective heat flux/corresponding conduction heat flux) increases with increasing external Rayleigh number and decreasing internal Rayleigh number. Along the hot surface, the behaviour of the average heat flux ratio is non-monotonic in nature. The heat flux ratio along both surfaces is observed to be strongly dependent on the inclination angle at high external Rayleigh numbers. A maximum in the local heat flux ratio along the cold surface is obtained in the vicinity of $x/L = 1$ where hot fluid, either from the interior or directly from the opposite hot wall, meets the surface. Along the hot wall, a maximum in the heat flux ratio is obtained near $x/L = 1$ or near $x/L = 0$ depending on whether the flow is downwards or upwards along the hot surface

Keywords: *convection, fluid mechanics, inclined enclosures*

Natural convection in both externally and internally heated enclosures has been extensively studied in the past. The published literature dealing with externally heated enclosures has been reviewed by Ostrach[1] and more recently by Catton[2]. The literature related to internally heated enclosures has been compiled recently[3].

Natural convection in an enclosure subjected to simultaneous internal heating and heating or cooling from below has received rather limited attention[4-10], with the horizontal layer being the only geometry considered. Baker, Faw and Kulacki[4] and Cheung[5] have each examined the available data for both internally heated layers with equal upper and lower boundary temperatures and internally heated layer with insulated lower boundary, and have presented correlations for internally heated layers with unequal boundary temperatures. Kikuchi, Kawasaki and Shiyoma[6] and Boon-Long, Lester and Faw[7] have investigated experimentally the heat transfer behaviour in a horizontal layer with simultaneous internal and external heating. Suo-Anttilla and Catton[8] have used the Landau method to determine the heat transfer in a horizontal, internally heated layer which is cooled from below and have conducted an experimental study of the same problem[9].

* Mechanical Engineering Department, Louisiana State University, Baton Rouge, Louisiana 70803, USA
Received 2 March 1984 and accepted for publication in its final form on 2 October 1984

As mentioned earlier, the published literature is primarily restricted to a horizontal layer. Recently, Acharya and Goldstein[10] have investigated the natural convection heat transfer in an inclined square box heated internally and from below. There is, however, no reported information on the heat transfer behaviour in an internally heated inclined enclosure which is cooled from below. Such a situation is analysed here.

A limiting case of the problem considered here is natural convection in an inclined enclosure cooled from below (with no internal energy sources). Solutions have been obtained for this case and compared with the results available in the literature[11-17].

Governing equations

In this study a Boussinesq fluid is considered. The natural convection motion is assumed to be steady, laminar and two-dimensional with the axes of the flow pattern parallel to the third dimension. For inclined enclosures cooled from below and for vertical enclosures, the two dimensional flow assumption has been established experimentally[13,18].

The physical situation to be considered is shown in Fig 1. The governing partial differential equations are the conservation of mass, momentum and energy which are non-dimensionalized using the following quantities:

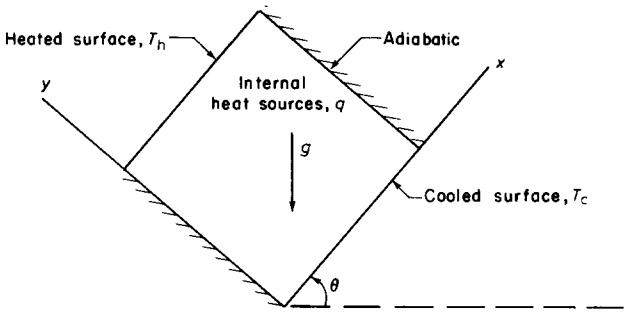

Fig 1 Schematic of the physical situation

$$X = x/L \qquad Y = y/L, \tag{1a}$$

$$U = u/(\nu/L) \qquad V = v/(\nu/L), \tag{1b}$$

$$P = p^*/\rho(\nu/L)^2 \text{ where } p^* = p + \rho g x \sin\theta + \rho g y \cos\theta \tag{1c}$$

$$\phi = (T - T_0)/(T_h - T_c) \text{ where } T_0 = (T_h + T_c)/2 \tag{1d}$$

The resulting equations are:

$$\partial U/\partial X + \partial V/\partial Y = 0 \tag{2}$$

$$U\partial U/\partial X + V\partial U/\partial Y = -\partial P/\partial X + \partial^2 U/\partial X^2 + \partial^2 U/\partial Y^2 + Ra_E \phi \sin\theta/Pr \tag{3}$$

$$U\partial V/\partial X + V\partial V/\partial Y = -\partial P/\partial Y + \partial^2 V/\partial X^2 + \partial^2 V/\partial Y^2 + Ra_E \phi \cos\theta/Pr \tag{4}$$

$$U\partial\phi/\partial X + V\partial\phi/\partial Y = (1/Pr)(\partial^2\phi/\partial X^2 + \partial^2\phi/\partial Y^2) + Ra_I/(Ra_E . Pr) \tag{5}$$

All four boundaries are considered to be rigid ($u = v = 0$) and the side walls are assumed to be adiabatic ($\partial\phi/\partial X = 0$). The lower wall ($y/L = 0$) is maintained at a temperature T_c (ie $\phi = -0.5$) while the upper wall ($y/L = 1$) is held at a temperature T_h (ie $\phi = 0.5$). Here T_c is assumed to be smaller than T_h.

It can be seen that there are five governing parameters in the problem: the external Rayleigh number Ra_E, the internal Rayleigh number Ra_I, the angle of inclination θ, the aspect ratio (H/L) and the Prandtl number Pr. Results are presented for Ra_E and Ra_I values of up to 10^6 and inclination angles of 90†, 60 and 30 degrees. Pr is assigned a constant value of 0.7 and the aspect ratio is assumed to be unity.

Note that the use of Boussinesq assumption implies that compressibility effects are small, which is justified[19] for $(T_h - T_c)/T_c < 0.2$. Also, since the influence of radiation and thermophysical property variations are not considered, the results reported in the paper are limited to small overall temperature differences.

Solution procedure

The governing partial differential equations are solved by using a control-volume based finite difference procedure called SIMPLER (Semi Implicit Method for Pressure Linked Equations Revised). This method has been accorded a book length description by Patankar[20] and, therefore, will not be described here.

A 32 × 32 grid is employed in all the calculations. The distribution of the nodal points is carefully tailored so that the solutions obtained are reasonably accurate. As a first step, the accuracy of the computed results was verified by determining whether overall energy conservation is satisfied. In dimensionless form, this requirement can be expressed as:

$$R = \frac{\int_{X=0}^{1} (-\partial\phi/\partial Y)_{Y=0}\,dx + Ra_I/Ra_E}{\int_{X=0}^{1} (-\partial\phi/\partial Y)_{Y=1}\,dx} = 1.0 \tag{6}$$

For all cases studied, R differs from 1.0 in only the third or fourth significant digit after the decimal point.

† Results for $\theta = 90°$ are taken from earlier work[10]

Notation

g	Gravitational acceleration
H	Height of enclosure
L	Width of enclosure
p, p^*, P	Thermodynamic, modified and dimensionless pressures
Pr	Prandtl number
Q	Uniform volumetric heat generation rate
q_s	Convective heat flux at the hot or cold surface
q_c	Conduction heat flux at the hot or cold surface, $-k(T_h - T_c)/L \mp QL/2$
$q_{r,h}$, $\bar{q}_{r,h}$	Heat flux ratio (q_s/q_c) at the hot surface and the corresponding average value
$q_{r,c}$, $\bar{q}_{r,c}$	Heat flux ratio (q_s/q_c) at the cold surface and the corresponding average value
R	Ratio defined in Eq (6)
Ra_E	External Rayleigh number, $g\beta(T_h - T_c)L^3/\nu\alpha$
Ra_I	Internal Rayleigh number, $g\beta QL^5/\nu\alpha k$
T	Temperature
T_h, T_c	Temperature of the hot and cold surfaces
T_0	Mean temperature, $(T_h + T_c)/2$
u, U	Dimensional and dimensionless velocities in the x-direction
v, V	Dimensional and dimensionless velocities in the y-direction
x, X	Dimensional and dimensionless coordinate along hot and cold wall
y, Y	Dimensional and dimensionless coordinate along adiabatic walls
α	Thermal diffusivity
β	Thermal expansion coefficient
θ	Angle of inclination
ν	Kinematic viscosity
ρ	Density
ϕ	Dimensionless temperature, $(T - T_0)/(T_h - T_c)$
ψ	Dimensionless stream function

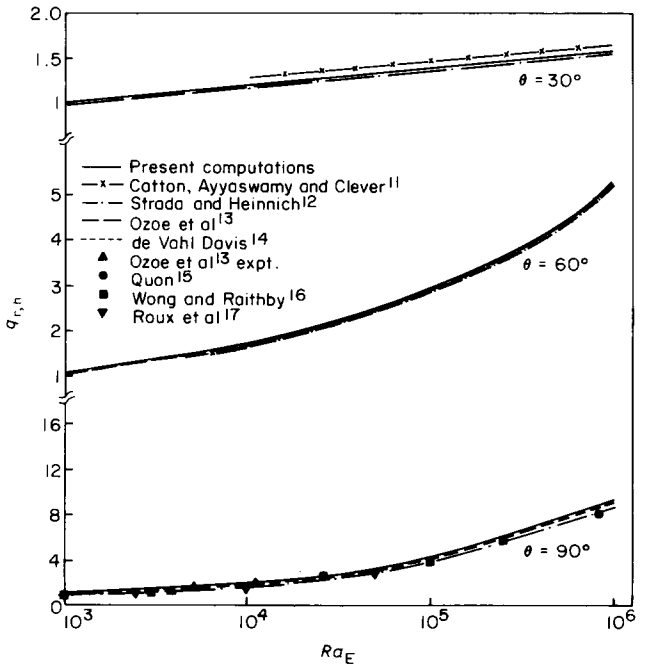

Fig 2 Comparison of predictions (of average heat flux ratio) with published results for an inclined enclosure cooled from below

Furthermore, the accuracy of the computed results in the absence of internal heating is demonstrated by comparing the computed results with those published in the literature (Fig 2). These predictions agree well with predictions and measurements published in the literature. The adequacy of the grid, in the presence of internal heating, is also verified by comparing the results computed with a 32×32 grid with those obtained using a 64×64 grid. This comparison, for the x-component of velocity along the centre line and the local Nusselt number along the hot surface is shown in Fig 3. Agreement is good and the other quantities show similar agreement. For example, the maximum x-velocity for the two grid sizes agrees to within 1.6%, the maximum temperature to within 0.6% and the average Nusselt number along the hot surface agrees to the fourth significant digit beyond the decimal point.

Results and discussion

The presentation of the results will begin with the streamline and isotherm patterns in the enclosure. Representative distributions of the average and local heat flux ratio will then be presented.

Streamline and isotherm pattern

The stream function ψ is calculated from the velocity field by evaluating the integral:

$$\psi = \int_0^Y U \, dY \tag{7}$$

along constant X lines with $\psi = 0$ at $X = Y = 0$.

For $\theta = 60°$, the streamline contours are shown in Figs 4–7. Fig 4 corresponds to Ra_I and Ra_E values of 0 and 10^6 respectively and indicates the presence of a base flow along the enclosure walls and secondary and tertiary eddies in the inner core. The base flow is expectedly upwards along the hot plate and downwards along the cold one. Both the secondary eddies have the same flow direction as the base flow (ie clockwise) while the tertiary eddy rotates in a direction opposite to the direction of the base flow. Both the streamline and isotherm contours reveal essential differences when compared with the corresponding contours for the bottom heated enclosure[10]. In the bottom-heated situation, velocity and temperature boundary layers were obtained over the entire thermally active surface. Here large velocity and temperature gradients occur only along the leading region of the hot surface (ie close to $x/L = 0$) and along the leading region of the cold surface (ie in the neighbourhood of $x/L = 1$). The magnitude of the gradients decreases rapidly in the flow direction. Furthermore, the flow velocities are smaller than the corresponding flow field velocities for the bottom-heated enclosure. This is expected since the bottom-heated configuration is more unstable than an enclosure heated from the top.

If the internal Rayleigh number is much larger than the external Rayleigh number, the flow pattern has a different nature. This is illustrated in Fig 5 for $Ra_I = 10^5$ and $Ra_E = 10^3$. The fluid rises in the interior and moves down both the hot and cold surfaces. The region of highest temperature is between the hot and cold walls and, therefore, the heat flux along both these walls is directed from the fluid to the wall. In contrast, for the situation shown in Fig 4 (ie where $Ra_I = 0$ or where the effect of Ra_E is dominant), the maximum temperature occurs at the hot surface with the heat flux at the cold surface directed from

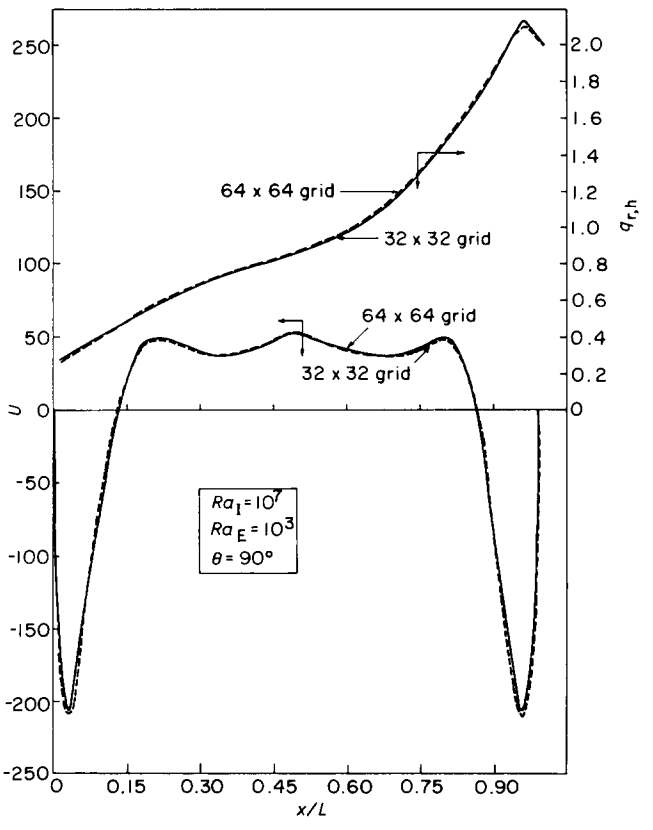

Fig 3 Comparison of local results for a 32×32 grid with the results for a 64×64 grid

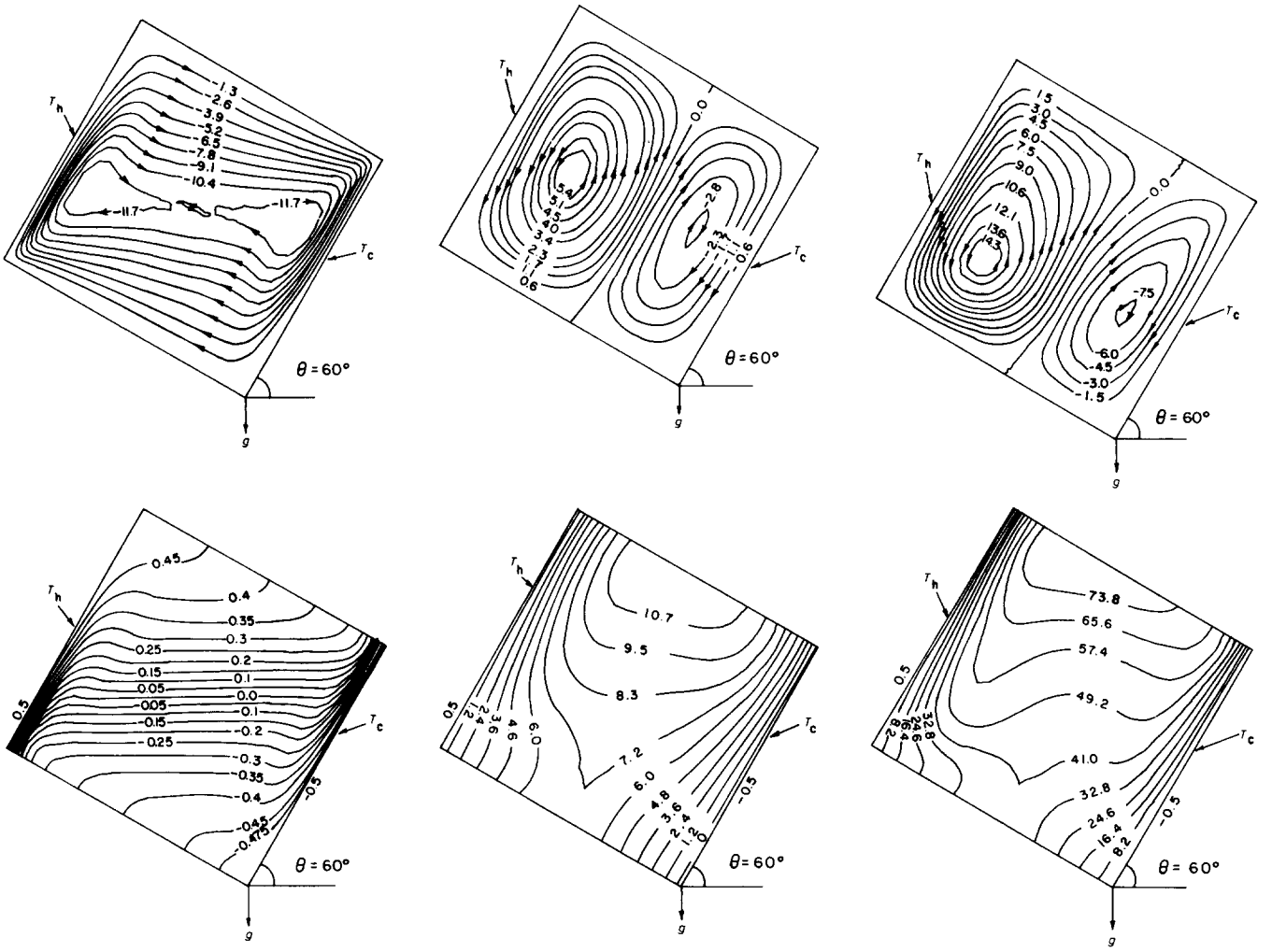

Fig 4 Contour plots for an inclined ($\theta = 60°$) enclosure, $Ra_I = 0$, $Ra_E = 10^6$: (top) streamline; (below) isotherm

Fig 5 Contour plots for an inclined ($\theta = 60°$) enclosure, $Ra_I = 10^5$, $Ra_E = 10^3$: (top) streamline; (below) isotherm

Fig 6 Contour plots for an inclined ($\theta = 60°$) enclosure, $Ra_I = 10^6$, $Ra_E = 10^3$: (top) streamline; (below) isotherm

the fluid to the wall and at the hot surface from the wall to the fluid.

At a constant Ra_E (smaller than Ra_I), if Ra_I is increased, say from 10^5 (Fig 5) to 10^6 (Fig 6), then the vigour of the downward flow is observed to increase over both the hot and cold surfaces. This is expected, since a higher value for Ra_I implies higher interior temperatures and therefore larger temperature gradients. If Ra_I is held fixed (at 10^6) and Ra_E increased from 10^3 to higher values, then, over a certain range of Ra_E the flow pattern undergoes a transition from that shown in Fig 6 (for $Ra_I = 10^6$, $Ra_E = 10^3$) to a flow pattern similar to that shown in Fig 4 (for $Ra_I = 0$, $Ra_E = 10^6$).

A transitional flow pattern is shown in Fig 7 (for $Ra_I = 10^6$ and $Ra_E = 10^5$). Compared to Fig 6, both the size and speed of the downward flow along the hot surface (counter-clockwise eddy) has decreased but the size of the downward flow along the cold surface (clockwise eddy) has increased. Note that the downward flow along the hot surface does not span the entire height of the enclosure, as it does when Ra_I is dominant, and therefore, along the hot surface the flow has both positive x velocities (due to the clockwise eddy) and negative x velocities (due to the counter-clockwise eddy). For a higher value of Ra_E, the counter-clockwise eddy is even smaller in size and eventually, at a sufficiently high value of Ra_E, the counter-clockwise eddy is completely absent and the flow is upwards along the heated wall and downwards along the cooled wall (as in Fig 4).

The flow pattern at $Ra_I = 0$ and $Ra_E = 10^6$ for an enclosure inclined at 30° is shown in Fig 8. When this flow pattern is compared with the corresponding flow field for $\theta = 60°$ (Fig 4) it can be observed that both flow patterns consist of a base flow (in a clockwise direction) adjacent to the enclosure walls and two secondary eddies (also rotating in a clockwise direction) and a tertiary eddy (rotating in a counter-clockwise direction) in the inner core. For $\theta = 60°$, however, the base flow occupies most of the enclosure cross-section while for $\theta = 30°$ the base flow is confined only to the near-wall region and it is the secondary eddies which occupy most of the enclosure cross-section. Furthermore, the flow velocities are smaller at $\theta = 30°$ than at $\theta = 60°$. This is expected since the buoyancy component parallel to the hot and cold surface is smaller (by a factor of 1.73) when the enclosure is inclined at 30° than when it is inclined at 60°.

The tertiary eddy obtained at the centre of the enclosure is due to the interaction of the secondary eddies. In Fig 8 it can be observed that the secondary eddies interact with the base flow (along the enclosure walls) and therefore, entrain the base flow along the region between the secondary eddies. The base flow entrained towards the

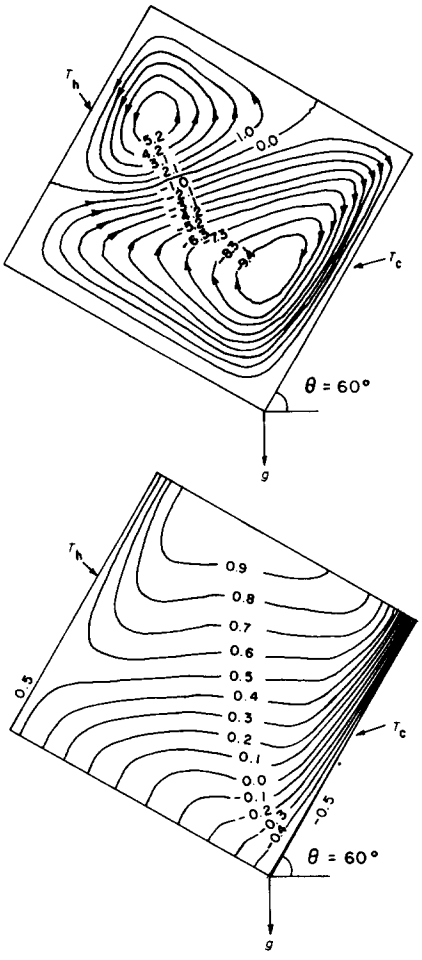

Fig 7 Contour plots for an inclined ($\theta = 60°$) enclosure, $Ra_I = 10^4$, $Ra_E = 10^5$: (top) streamline; (below) isotherm

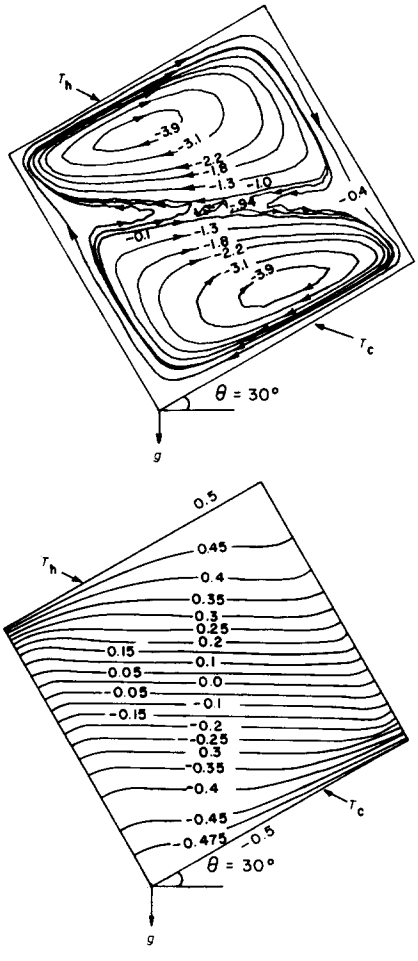

Fig 8 Contour plots for an inclined ($\theta = 30°$) enclosure, $Ra_I = 0$, $Ra_E = 10^6$: (top) streamline; (below) isotherm

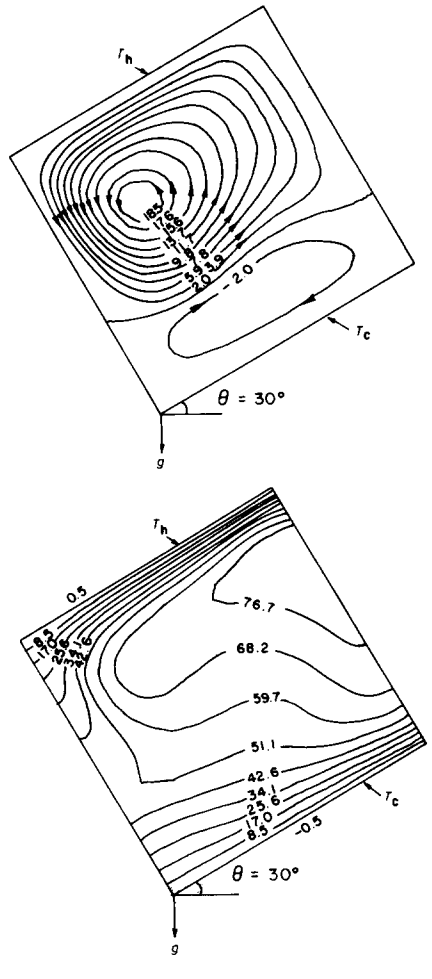

Fig 9 Contour plots for an inclined ($\theta = 30°$) enclosure, $Ra_I = 10^6$, $Ra_E = 10^3$: (top) streamline; (below) isotherm

centre of the enclosure by the secondary eddy moving down the cold surface, or by the secondary eddy moving up the hot surface, experiences a retarding shear force by the other secondary eddy. Therefore, the velocity of the entrained fluid continuously decreases along the direction of its motion and eventually its flow direction is reversed. The location of flow reversal is marked by the onset of tertiary motion.

The isotherm pattern in Fig 8 indicates the absence of thermal boundary layers along the hot and cold surface. Thus, by comparing the flow and isotherm patterns (for $Ra_I = 0$) at $\theta = 30°$ (Fig 8), $\theta = 60°$ (Fig 4) and $\theta = 90°$ (Ref 10), it may be concluded that the boundary layer behaviour at the hot and cold walls decreases as the inclination angle is decreased.

As at $\theta = 60°$, if the internal Rayleigh number is considerably larger than the external Rayleigh number (eg $Ra_I = 10^6$, $Ra_E = 10^3$) then the flow pattern has a different nature, with fluid moving upwards in the interior of the enclosure and moving down both the hot and cold walls (Fig 9). In comparing Fig 9 ($\theta = 30°$) with Fig 6 ($\theta = 60°$), it may be observed that the downward flow along the cold surface is weaker and the downward flow along the hot surface is stronger at $\theta = 30°$ than at $\theta = 60°$. This is because the x-component of buoyancy due to external heating opposes the flow due to internal heating moving down the hot surface and aids the flow due to internal heating moving down the cold surface. At $\theta = 30°$ the x-component of buoyancy due to external heating is smaller than the corresponding value at $\theta = 60°$. Therefore, the flow down the hot surface is stronger and the flow down the cold surface is weaker at $\theta = 30°$ than at $\theta = 60°$.

With Ra_I fixed (at 10^6), if Ra_E is increased from 10^3 (Fig 9) to 10^5 (Fig 10), the downward flow over the cold surface increases in size and becomes faster while the downward flow over the hot surface is reduced in size and becomes slower. This behaviour is once again linked to the fact that with increasing Ra_E values, the magnitude of the x-component of buoyancy is increased and therefore aids the downward flow along the cold surface and opposes the downward flow along the hot surface.

As mentioned earlier, if Ra_I is held fixed and Ra_E is increased (from a value smaller than Ra_I) then, over a certain range of Ra_E values, the flow pattern changes from one where the flow moves downwards over both hot and cold surfaces to one where the flow moves upwards along the hot surface and downwards along the cold surface. This transition in flow pattern is obtained at a lower value of Ra_E when the inclination angle of the enclosure is larger (ie 60°). To substantiate this conclusion, Fig 7 ($\theta = 60°$, $Ra_I = 10^6$ and $Ra_E = 10^5$) is compared with Fig 10 ($\theta = 30°$, $Ra_I = 10^6$ and $Ra_E = 10^5$). In Fig 10 ($\theta = 30°$) the flow moving down the cold wall occupies less than half the enclosure cross-section and is weaker than the flow

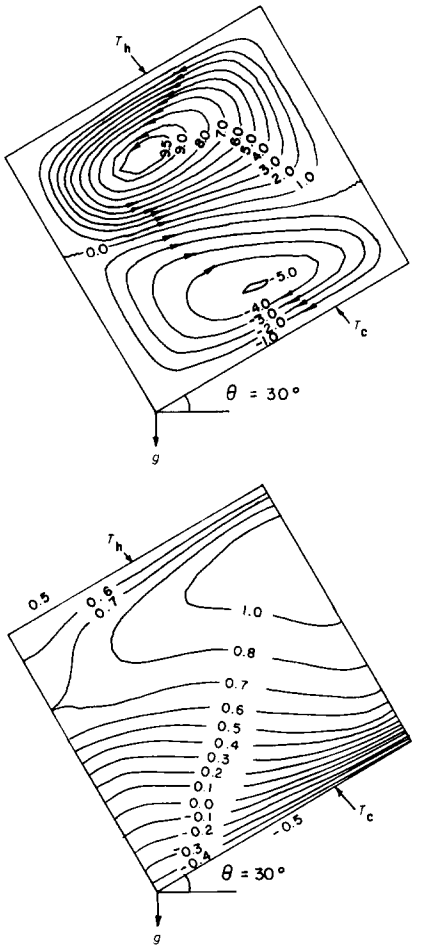

Fig 10 Contour plots for an inclined ($\theta=30°$) enclosure, $Ra_I=10^6$, $Ra_E=10^5$: (top) streamline; (below) isotherm

moving down the hot wall. In Fig 7 ($\theta=60°$) the flow moving down the cold wall occupies most of the enclosure cross-section and is considerably stronger than the flow moving down the hot wall. Therefore, the transition in the flow pattern has progressed substantially further with the enclosure inclined at 60° than with the enclosure inclined at 30°.

Average heat flux ratios

To describe the heat transfer behaviour in the enclosure, a heat flux ratio is defined for both the cold ($q_{r,c}$) and the hot ($q_{r,h}$) surfaces:

$$q_{r,c}=(q_s/q_c)_{y=0}, \tag{8a}$$

$$q_{r,h}=(q_s/q_c)_{y=L}. \tag{8b}$$

where q_s is the surface heat flux (in the positive y direction) and q_c is the corresponding conduction heat flux (at the same value of Q and (T_h-T_c)). When expressed in dimensionless terms, Eq (8) takes the form:

$$q_{r,c}=(-\partial\phi/\partial Y)_{Y=0}/(1+0.5Ra_I/Ra_E), \tag{9a}$$

$$q_{r,h}=(-\partial\phi/\partial Y)_{Y=1}/(1-0.5Ra_I/Ra_E). \tag{9b}$$

The average heat flux ratios $\bar{q}_{r,c}$ and $\bar{q}_{r,h}$ are obtained by averaging the local heat flux ratios $q_{r,c}$ and $q_{r,h}$.

The average heat flux ratio along the cold surface ($\bar{q}_{r,c}$) for an inclination of 60° (Fig 11) increases monotonically with increasing Ra_E because the strength of the downward flow (and therefore the surface heat flux) along the cold surface increases with increasing Ra_E.

At a fixed Ra_E, the magnitude of $\bar{q}_{r,c}$ is observed to decrease with increasing Ra_I. This implies that for a certain increase in the value of Ra_I (ie the strength of the internal heat sources), the increase in the average value of the convective heat transfer at the cold surface (ie q_s at $y=0$) is smaller than the corresponding increase of the conduction heat flux.

The convective heat transfer at the cold surface is dictated by a number of interacting effects. To explain these effects the situation for which Ra_I is much greater than Ra_E is first considered. In this case, the flow is downwards over both the hot and cold surfaces. Hot interior fluid is carried in a clockwise direction to the cold surface resulting in higher heat transfer rates, compared to the conduction value, in the vicinity of the leading edge of cold surface ($x/L=1$). As the fluid moves over the cold surface, its temperature decreases and, therefore, both the temperature gradient and the surface heat flux decrease. Moreover, the hot interior fluid is cooled by the downward flow along the hot surface and therefore the temperature gradient at the cold surface decreases. The cumulative influence of these effects decides the value of the surface heat flux. For Ra_I values of 10^4, 10^5 and 10^6, there is a range of Ra_E values ($\ll Ra_I$) for which the average convection heat transfer at the cold surface is smaller than the corresponding conduction value (ie $\bar{q}_{r,c}<1$).

When $Ra_E>Ra_I$, the flow moves up the hot wall and down the cold wall. As Ra_E is increased, the influence of internal heating on the heat transfer at the cold surface is reduced. Therefore, with increasing Ra_E, the $\bar{q}_{r,c}$ values approach those predicted for zero Ra_I.

The influence of inclination angle on the average heat flux ratio along the cold surface is shown in Fig 12. For $Ra_I=0$ and 10^5, results for a vertical enclosure ($\theta=90°$) have been obtained from earlier work[10].

For all three Ra_I values (0, 10^5 and 10^6), $\bar{q}_{r,c}$ has a higher value at a larger angle of inclination. Furthermore,

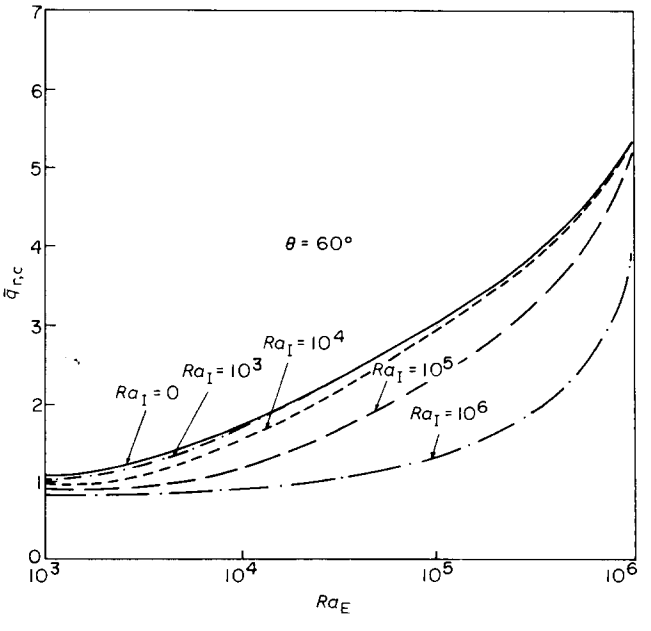

Fig 11 Average heat flux ratio along the cold surface for an inclination of 60°

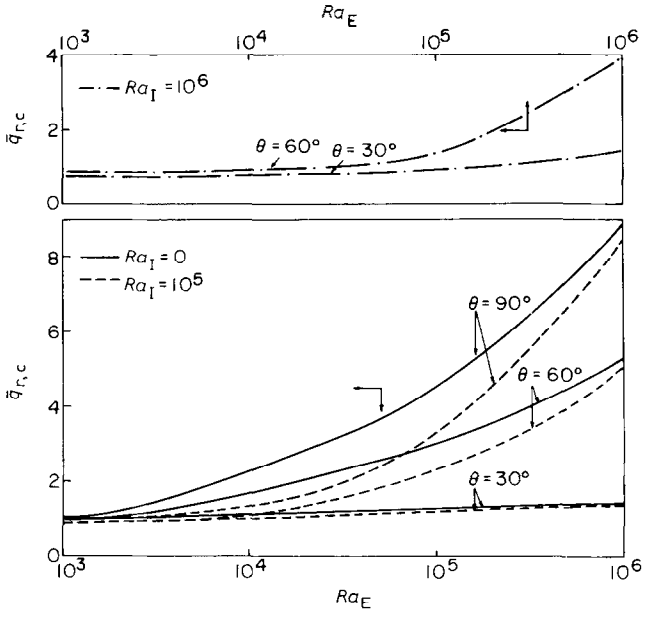

Fig 12 Dependence of the average heat flux ratio along the cold surface on inclination angle

the influence of inclination angle increases as Ra_E increases. At $Ra_I = 10^5$ and $Ra_E = 10^6$, $\bar{q}_{r,c}$ for $\theta = 90°$ is approximately 1.65 times the corresponding value for $\theta = 60°$ and 5.5 times the predicted value for $\theta = 30°$. For smaller Ra_E (10^3 and 10^4) the differences in the predicted $\bar{q}_{r,c}$ values are substantially smaller.

To explain these trends, note that for large Ra_E values the flow is upwards along the hot wall and downwards along the cold wall. As the enclosure is inclined towards the horizontal, the flow field becomes increasingly thermally stratified resulting in smaller velocities and lower heat transfer. For Ra_E less than Ra_I, the flow is downwards along both the hot and cold surfaces with the flow along the cold surface becoming faster with increasing inclination from the horizontal. Therefore, as in the case of large Ra_E, a higher value of $\bar{q}_{r,c}$ is obtained at a larger inclination angle.

Turning to the distribution of the average heat flux ratio along the hot surface (Fig 13), from Eq (9b) it can be seen that $q_{r,h}$ becomes singular at $Ra_E = 0.5Ra_I$. At this value of Ra_E, the conduction heat flux q_c at the hot surface is zero since the contribution (to q_c) due to external heating exactly cancels the contribution due to the internal energy sources. In the neighbourhood of this singularity the behaviour of $q_{r,h}$ is expected to be quite irregular with its magnitude increasing rapidly to infinity (as Ra_E tends to the singularity value of $0.5Ra_I$) and then decreasing rapidly from infinity (as the singularity is crossed). Therefore, since the results have been obtained only for Ra_E values of 10^3, 10^4, 10^5 and 10^6 (and not in the immediate vicinity of the singularity), the $\bar{q}_{r,h}$ curve in the neighbourhood of the singularity has been intentionally omitted. It should be noted that the Ra_E range in which the flow transition discussed above occurs, and in which the convective flux at the hot surface increases from a negative value to zero and then to a positive value, is approximately the same as the Ra_E range in which $q_{r,h}$ behaviour is irregular and in which conduction heat flux at the hot surface increases from a negative value to zero and then to a positive value.

Fig 13 shows that for $Ra_I = 0$ (and 10^3) $\bar{q}_{r,h}$ increases with Ra_E. As for $\bar{q}_{r,c}$, this behaviour is explained by noting that the strength of the flow moving upwards along the hot surface increases with increasing Ra_E. For $Ra_E \ll Ra_I$, the flow is downwards along both the hot and cold surface. For such situations $\bar{q}_{r,h}$ is smaller than the corresponding predictions for $Ra_I = 0$ and even drops below the conduction value of 1. As for the cold surface, the magnitude of $\bar{q}_{r,h}$ is an outcome of a number of interacting effects. High heat transfer rates are obtained when the internally heated fluid rises in the interior and encounters the leading edge ($x/L = 1$) of the hot surface. The flow is cooled as it moves down the hot surface and therefore, the heat transfer rate decreases. Furthermore, the interior flow is cooled by the cold wall and therefore results in lower temperature gradients at the hot surface.

For Ra_E greater than Ra_I, the transition in flow pattern (from flow down the hot surface to flow up the hot surface) is complete and the strength of the upward flow along the hot surface increases as Ra_E is increased. Therefore, the $\bar{q}_{r,h}$ values increase and as Ra_E becomes sufficiently large (and the influence of Ra_I decreases) the $\bar{q}_{r,h}$ curve approaches that predicted for zero Ra_I.

The influence of inclination angle on the $\bar{q}_{r,h}$ distribution is shown in Fig 14. Results are presented only for $Ra_I = 10^5$. The results for $Ra_I = 10^6$ show similar trends and the results for $Ra_I = 0$ are identical to those plotted in Fig 12.

Note that the inclination angle has a strong influence at large Ra_E, but only a weak influence at small Ra_E. At large Ra_E, the flow is upwards along the hot surface and, as mentioned earlier, becomes faster at a higher inclination angle. Thus, higher values of $\bar{q}_{r,h}$ are obtained at a larger inclination angle. This trend is completely reversed at the smaller Ra_E values. For these situations, the flow is downwards over the hot surface. As the inclination angle becomes larger, the strength of the downward flow over the cold surface increases producing greater cooling in the interior. However, the strength of the downward flow over the hot surface decreases. The net effect is lower interior temperatures and smaller temperature gradients at the hot surface. Therefore, for small Ra_E values, $\bar{q}_{r,h}$ decreases with increasing angle.

Fig 15 plots the local heat flux ratio along the hot and cold surfaces for two different sets of Rayleigh

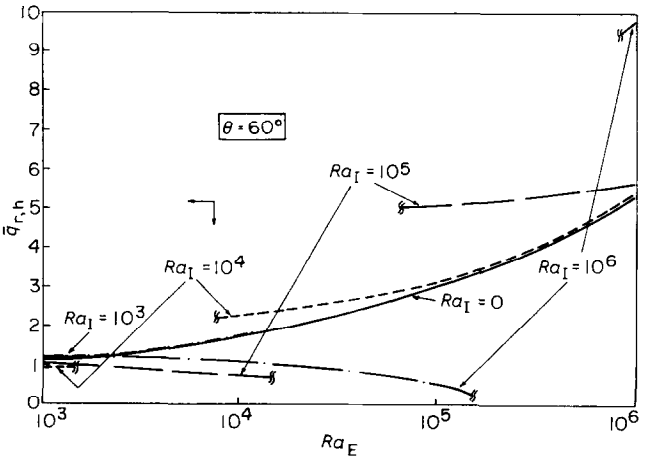

Fig 13 Average heat flux ratio along the hot surface for an inclination of 60°

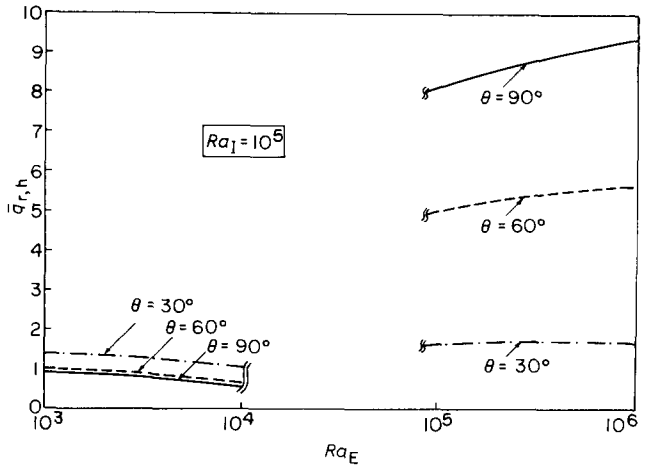

Fig 14 Dependence of the average heat flux ratio along the hot surface on inclination angle

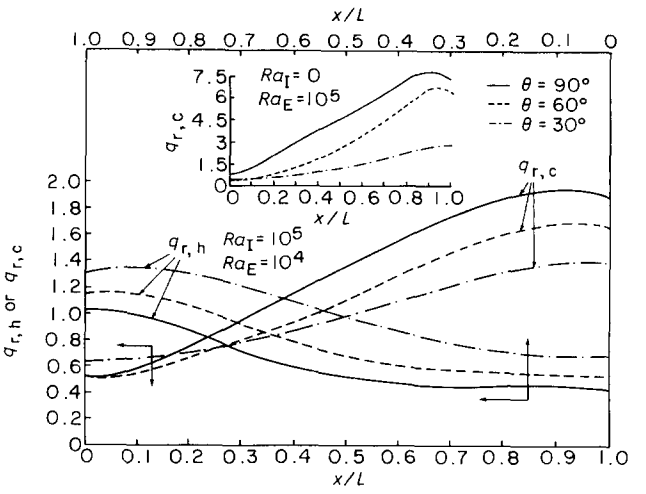

Fig 15 Local heat flux ratio along the hot and cold surfaces

numbers and for all three inclination angles. The inset of Fig 15 plots the distribution of $q_{r,c}$ for $Ra_I = 0$ and $Ra_E = 10^5$. In the neighbourhood of $x/L = 1$, heated fluid from the hot surface of the enclosure meets the lower cold wall and thus large $q_{r,c}$ values are obtained. As the fluid moves down the cold surface, its temperature decreases and therefore, both the temperature gradient and $q_{r,c}$ decrease. As explained before, the $q_{r,c}$ value is higher at 90° than at 60° and 30°. This discrepancy is largest in near $x/L = 1$ (where the wall to adjacent fluid temperature difference is large) and the smallest near $x/L = 0$ (where the wall to adjacent fluid temperature difference is small). Thus, the decrease in $q_{r,c}$ value as the flow moves down the cold surface is greater for a vertical enclosure than it is for an inclined enclosure.

The distribution of $q_{r,h}$ (for $Ra_I = 0$) is identical to that shown for $q_{r,c}$ with the x/L along the lower abscissa replaced by $(1 - x/L)$.

For $Ra_I = 10^5$ and $Ra_E = 10^4$, the distribution for $q_{r,h}$ is keyed to the abscissa on the top of the plot while that for $q_{r,c}$ is keyed to the abscissa along the bottom of the plot. As expected, for both the hot and cold surfaces, the maximum heat flux ratio is obtained in the neighbourhood of the location where the hot interior fluid meets the thermally active surfaces, ie near $x/L = 1$. As the fluid flows down (from $x/L = 1$ towards $x/L = 0$) the hot (or cold) surface, its temperature decreases thus resulting in smaller temperature gradients and heat flux ratios. $q_{r,h}$ decreases but $q_{r,c}$ increases with increasing angle as a result of the decreasing strength of the downward flow along the hot surface and the increasing strength of the downward flow along the cold surface with increasing angle.

In general, the angle of inclination has a considerably greater influence on the overall heat transfer rate when the enclosure is cooled from the bottom than when it is heated from the bottom[10].

Concluding remarks

Natural convection in an inclined enclosure cooled from below and containing internal energy sources has been investigated by a finite-difference procedure. Results indicate that for $Ra_E > Ra_I$, the flow is upwards along the hot wall and downwards along the cold wall. For values of Ra_E which are considerably smaller than Ra_I, the flow rises up in the interior and moves down both the hot and cold walls. For intermediate Ra_E values ($0.1Ra_I < Ra_E < Ra_I$) transitional flow patterns are observed. The average heat flux ratio along the cold surface increases with increasing Ra_E and decreasing Ra_I. The average heat flux ratio along the hot surface exhibits non-monotonic behaviour for non-zero Ra_I with large variations in the Ra_E range associated with the transition in the flow pattern. At high Ra_E values, the inclination angle has a strong influence on the magnitude of the heat flux ratio. The maximum heat flux ratio along the cold surface occurs near $x/L = 1$ while along the hot surface it occurs near $x/L = 0$ if the flow is upwards along the hot surface and near $x/L = 1$ if the flow is downwards along the hot surface.

References

1. **Ostrach S.** Natural Convection in Enclosures. in *Advances in Heat Transfer, (eds. J. P. Hartnett and T. F. Irvine) 1972*, **8**, *161–227*
2. **Catton I.** Natural Convection in Enclosures. *Proc. 6th Int. Heat Transfer Conf., 1978*, **2**, *13–31*
3. **Kulacki F. A., Catton I., Chen C. F. and Edwards D. K.** Fluid Layers. *Proc. of a Workshop on Natural Convection, (eds. K. T. Yang and J. R. Lloyd) July 18–21, 1982, Breckenridge, Colorado*
4. **Baker L., Faw R. E. and Kulacki F. A.** Post Accident Heat Removal – Part 1: Heat Transfer Within an Internally Heated, Non-boiling Liquid Layer. *Nucl. Sci. Eng., 1976*, **61**, *222–230*
5. **Cheung F. B.** Correlation Equation for Turbulent Thermal Convection in a Horizontal Layer Heated Internally and From Below. *J. Heat Transfer, 1978*, **100**, *416–422*
6. **Kikuchi Y., Kawasaki T. and Shiyoma T.** Thermal Convection in a Horizontal Fluid Layer Heated Internally and From Below. *Int. J. Heat Mass Transfer, 1982*, **25**, *363–370*
7. **Boon-Long P., Lester T. W. and Faw R. E.** Convective Heat Transfer in an Internally Heated Horizontal Fluid Layer with Unequal Boundary Temperatures. *Int. J. Heat Mass Transfer, 1979*, **22**, *437–445*
8. **Suo-Anttila A. J. and Catton I.** The Effect of a Stabilizing Temperature Gradient on Heat Transfer from a Molten Fuel Layer with Volumetric Heating. *J. Heat Transfer, 1975*, **97**, *544–548*
9. **Suo-Anttila A. J. and Catton I.** An Experimental Study of a Horizontal Layer of Fluid with Volumetric Heating and Unequal

Surface Temperatures. *Paper No. AICHE-5, 16th National Heat Transfer Conference, St. Louis, 1976*

10. **Acharya S. and Goldstein R. J.** Natural Convection in an Externally Heated Vertical or Inclined Square Box Containing Internal Energy Sources. *ASME/AICHE National Heat Transfer Conference, Seattle, July 24–28, 1983*

11. **Catton I., Ayyaswamy P. S. and Clever R. M.** Natural Convection Flow in a Finite, Rectangular Slot Arbitrarily Oriented with Respect to the Gravity Vector. *Int. J. Heat Mass Transfer, 1974,* **17**, *173–184*

12. **Strada M. and Heinrich J. C.** Heat Transfer Rates in Natural Convection at High Rayleigh Numbers in Rectangular Enclosures: A Numerical Study. *Numerical Heat Transfer, 1982,* **5**, *81–93*

13. **Ozoe H., Sayama H. and Churchill S. W.** Natural Convection in an Inclined Square Channel. *Int. J. Heat Mass Transfer, 1974,* **17**, *401–406*

14. **de Vahl Davis G.** Natural Convection of Air in a Square Cavity. A Bench Mark Solution. *Report 1982/FMT/2, School of Mechanical and Industrial Engr., Univ. of New South Wales, April 1982*

15. **Quon C.** High Rayleigh Number Convection in an Enclosure – A Numerical Study. *Physics of Fluids, 1972,* **15**, *12–19*

16. **Wong H. H. and Raithby G. D.** Improved Finite Difference Methods Based on a Critical Evaluation of the Approximation Errors. *Numerical Heat Transfer, 1979,* **2**, *139–163*

17. **Roux B., Grondin J. C., Bontoux P. and Gilly B.** On a High Order Accurate Method for the Numerical Study of Natural Convection in a Vertical Square Cavity. *Numerical Heat Transfer, 1978,* **1**, *331–349*

18. **Arnold J. N., Catton I. and Edwards D. K.** Experimental Investigation of Natural Convection in Inclined Rectangular Regions of Differing Aspect Ratios. *J. Heat Transfer, 1976,* **98**, *67–98*

19. **Zhong Z. Y.** Variable Property Natural Convection and its Interaction with Thermal Radiation. *Ph.D. Thesis, Department of Aerospace and Mechanical Engineering, University of Notre Dame, Indiana, 1983*

20. **Patankar S. V.** Numerical Heat Transfer, *Hemisphere, 1980*

BOOK REVIEW

Perturbation Methods in Heat Transfer

A. Aziz and T. Y. Na

The authors have produced a volume that they assert is both 'a textbook and an up-to-date reference' on perturbation methods applied to heat transfer problems. The book was published in 1984 and the most recent reference cited is 1982, so the last claim may be justified. I am less certain of the value of the work as a textbook, but it may be a useful reference in some cases. The subject matter of the book places it beyond most undergraduates and all but a few beginning graduate students. A background in heat transfer and fluid mechanics is definitely needed.

Following an introductory chapter, the authors take up, in turn, regular and singular perturbation expansions, the method of strained coordinates, the method of matched asymptotic expansions, and techniques for improving the range of convergence of perturbation series. A bibliography of heat transfer literature in which perturbation techniques have been used completes the book.

As a rule, the mathematical analysis for a particular topic is introduced through an example with no particular physical significance. This is followed by several analyses of heat transfer problems that have been treated in the literature. In most instances, perturbation parameters are introduced without either mathematical or physical explanation and the reader is left to speculate on how they came about. Frequently, the problem statements are incomplete. Only rarely do the authors provide a physical interpretation of the parameters or the results. Occasionally, the interested reader will be forced to consult an original reference for this interpretation, for a clear problem statement and to check for errors that have been introduced. Heat transfer is a field where physical explanations can be used to enrich and explain a mathematical analysis. I am disappointed that the authors chose not to do so.

The text is generally clear, but it is replete with awkward grammatical constructions. The inappropriate use (or absence) of definite and indefinite articles causes some confusion.

The ordering of topics is good and the coverage is generally adequate. I believe that many readers will find this book a useful starting point for a more detailed study of perturbation methods. The references and the bibliography are complete enough so additional material can be located easily.

R. Eichhorn
University of Houston,
Texas, USA

Published, price $37.50, by Hemisphere/Springer-Verlag. Hemisphere Publishing Corporation, Berkeley Building, 19W 44th Street, New York, NY 10036, USA. Springer-Verlag, Heidelberger Platz 3, Postfach, D-1000 Berlin 33, FRG